ELSEVIER

Nuclear Physics A 706 (2002) 203–216

NUCLEAR PHYSICS A

www.elsevier.com/locate/npe

First measurement of the d(p, γ)^{3}He cross section down to the solar Gamow peak

LUNA Collaboration

C. Casella [a], H. Costantini [b], A. Lemut [b], B. Limata [c], R. Bonetti [a], C. Broggini [d], L. Campajola [c], P. Corvisiero [b], J. Cruz [e], A. D'Onofrio [f], A. Formicola [g], Z. Fülöp [h], G. Gervino [i], L. Gialanella [c], A. Guglielmetti [a], C. Gustavino [j], G. Gyurky [h], G. Imbriani [c], A.P. Jesus [e], M. Junker [j], A. Ordine [c], J.V. Pinto [e], P. Prati [b,*], J.P. Ribeiro [e], V. Roca [c], D. Rogalla [g], C. Rolfs [g], M. Romano [c], C. Rossi-Alvarez [d], F. Schuemann [g], E. Somorjai [h], O. Straniero [k], F. Strieder [g], F. Terrasi [f], H.P. Trautvetter [g], S. Zavatarelli [b]

[a] *Università di Milano, Istituto di Fisica and INFN, Milano, Italy*
[b] *Università di Genova, Dipartimento di Fisica and INFN, Genova, Italy*
[c] *Dipartimento di Scienze Fisiche, Università Federico II and INFN, Napoli, Italy*
[d] *INFN, Padova, Italy*
[e] *Centro de Fisica Nuclear da Universidade de Lisboa, Lisboa, Portugal*
[f] *Dipartimento di Scienze Ambientali, Seconda Università di Napoli, Caserta and INFN, Napoli, Italy*
[g] *Institut für Physik mit Ionenstrahlen, Ruhr-Universität Bochum, Bochum, Germany*
[h] *Atomki, Debrecen, Hungary*
[i] *Universita' di Torino, Dipartimento di Fisica Sperimentale and INFN, Torino, Italy*
[j] *Laboratori Nazionali del Gran Sasso, INFN, Assergi, Italy*
[k] *Osservatorio astronomico di Teramo, Teramo, Italy*

Received 12 December 2001; received in revised form 6 February 2002; accepted 26 February 2002

Abstract

Using the 50 kV LUNA accelerator facility at the Gran Sasso underground laboratory we measured, with an accuracy of the order of 10%, the d(p, γ)^{3}He cross section from 22 down to

* Corresponding author. Address: Dipartimento di Fisica, via Dodecaneso 33, 16146, Genova, Italy.
E-mail address: prati@ge.infn.it (P. Prati).

0375-9474/02/$ – see front matter © 2002 Elsevier Science B.V. All rights reserved.
PII: S0375-9474(02)00749-2

2.5 keV c.m. energy, well below the solar Gamow peak. The experimental set-up was based on a large solid angle, segmented BGO detector and a renewed windowless gas target. The astrophysical $S(E)$ factor within the Gamow peak is in fair agreement with the value of one of the existing extrapolations of data at higher energies. © 2002 Elsevier Science B.V. All rights reserved.

PACS: 26.65.+t; 25.90.+k

Keywords: NUCLEAR REACTIONS ^{2}H (p, γ), $E = 4$–32 KeV; Measured σ, astrophysical S-factors

1. Introduction

It is well known that thermonuclear reactions provide the major source of energy in stars. In a typical low-mass star, like the Sun, it has been estimated that more than 98% of the radiated energy is produced via the p–p chain, according to which 4 protons are gradually converted into a ^{4}He nucleus together with 2 positrons and 2 neutrinos, with a net energy output of about 26 MeV. The key reaction is $\mathrm{p(p, e^{+}\nu)d}$, the bottleneck of the chain, that regulates the energy production, while other chain reactions influence the nucleosynthesis of light nuclei and the neutrino energy spectrum in low mass stars [1]. Therefore, precise measurements of the reaction rates are mandatory requirements for modern stellar astrophysics. Due to the Coulomb barrier of the entrance channel, the cross section $\sigma(E)$ drops nearly exponentially with decreasing center-of-mass energy E (in the text all energies are in the center-of-mass system except where quoted differently), thus becoming increasingly difficult to measure $\sigma(E)$ at the relevant energy at which the reaction takes place in stars (the Gamow peak). Instead, one was forced to extrapolate high-energy $\sigma(E)$ data to stellar energies using the astrophysical $S(E)$ factor defined by the equation

$$\sigma(E) = \frac{S(E)}{E} \mathrm{e}^{-2\pi\eta}, \tag{1}$$

where η is the Sommerfeld parameter, $2\pi\eta = 31.29 Z_1 Z_2 (\mu/E)^{1/2}$, Z_1 and Z_2, and μ is the reduced mass.

In order to reduce or eliminate the uncertainties behind extrapolation procedures, considerable efforts have been spent in recent years to push the experimental limits towards lower and lower energies. For example, the LUNA (Laboratory for Underground Nuclear Astrophysics) facility [2] was installed in the Laboratori Nazionali del Gran Sasso (LNGS) with the initial motivation of measuring the cross section of one of the key reactions, namely ^{3}He(^{3}He, 2p)^{4}He, in the energy range of its solar Gamow peak. To achieve this goal, the experimental sensitivity had to be increased by several orders of magnitude in comparison to previous work, both by optimizing accelerator performances and detection efficiency and by minimizing background contributions. The LUNA facility is a 50 kV accelerator characterized by compactness, small energy spread, and high beam current (a few hundred μA) [2]. Its unique feature, however, is the cosmic-ray background suppression provided by the 4000 meters water-equivalent shield of the Gran Sasso mountain, which allowed to measure $\sigma(E)$ as low as 0.01 pb [3].

In this paper we report the measurement of the cross section of $d(p,\gamma)^3He$, the second step of the p–p chain, as obtained with the LUNA facility. Since the rate of this reaction is high, with respect to that of the deuterium producer $p(p,e^+\nu)d$, it only affects the equilibrium abundance of deuterium in an H-burning low-mass star. However, well before the onset of the H-burning (during the so called pre-main sequence phase), an important d-burning takes place [4]. Reliable proto-star models predict that a star forms by accretion of interstellar material onto a small contracting core. Until the temperature remains below 10^6 K, the main source of energy is the gravitational contraction. On the basis of the virial theorem, one half of the gravitational energy is spent to supplying the surface energy loss, while the other half goes into heat. When the temperature approaches 10^6 K, the original deuterium (a mass fraction of about 2×10^{-5}) is converted in to ^{3}He via $d(p,\gamma)^3He$, thus providing 5.5 MeV for each reaction. The total amount of nuclear energy generated by this d-burning is comparable with the whole gravitational binding energy of the star. The main effect of the onset of d-burning is to slow down the contraction and, in turn, the heating. As a consequence, the lifetime of the star increases and its observational properties (surface luminosity and temperature) are frozen until the original deuterium is fully consumed. Due to the slow evolutionary time-scale, a large fraction of the proto-stars is actually observed during this d-burning phase and only a negligible amount is expected in the previous, more rapid, evolutionary phase. A reliable knowledge of the rate of $d(p,\gamma)^3He$ down to a few keV (the Gamow peak in a proto-star) is a fundamental prerequisite for these stellar models.

The $d(p,\gamma)^3He$ reaction is also a cornerstone in the big-bang nucleosynthesis, providing one of the to main channels of the ^{4}He production. In this case, however, the energy of the Gamow peak is high enough that measurements approaching the stellar energies are already available. Because of the relatively low height of the d + p Coulomb barrier, several experiments have been performed on this reaction which is believed to be dominated by the direct capture mechanism [1]. The reaction Q value is 5.5 MeV: with proton beams with energy E_p of few tens of keV, the energy of the emitted photon is $E_\gamma = Q + 0.67E_p$ and can be considered constant at 5.5 MeV within the typical energy resolution of scintillation detectors. A detailed discussion of the reaction mechanism is given in [5], where the cross section has been measured down to $E = 16$ keV. In a more recent work [6], an energy as low as $E = 10$ keV was reached. Both measurements do not overlap with the relevant Gamow peak in proto-stars and in the Sun (which extends from 3 to 10 keV); moreover, when extrapolated to zero energy, the astrophysical $S(0)$ factors deduced by the two groups exhibit a 40% discrepancy.

2. Experimental apparatus

The 50 kV LUNA accelerator at LNGS has been described elsewhere [2]. Briefly, it consists of a duoplasmatron ion source, an extraction/acceleration system, and a double focusing 90° analyzing magnet (with adjusted table pole faces). The energy spread of the ion source is less than 20 eV, the plasma potential energy deviates by less than 10 eV from the voltage applied to the anode, and the emittance of the source is about 2 cm rad $eV^{1/2}$. The ion source, even at the lowest extraction energies adopted for the experiment, provided stable proton beams with currents of few tens of μA for periods up to 50 hours. The High

Voltage (HV) power supply has a typical ripple of 5×10^{-5}, a long-term stability better than 1×10^{-4} and a temperature coefficient better than 1.5×10^{-4}/K. The HV of the accelerator, and therefore the beam energy, is measured with a resistor chain, contained in an air-tight plexiglass tube, and a digital multimeter. The resistor chain was built as a voltage divider, with fifty 20 MΩ resistors and one 100 kΩ resistor (temperature coefficient $= 1 \times 10^{-5}$/K). The multimeter (Hewlett Packard, model 3410) provided the numerical value of the HV measured across the 100 kΩ resistor. The resistor chain has been calibrated to a precision of 5×10^{-5} and the uncertainty in the beam energy is 10^{-4} [2].

We used a differentially pumped gas-target system designed to fit the characteristics of a large BGO gamma detector. Details of the technical solutions adopted for this new part of the set-up (gas target, beam calorimeter, BGO detector and acquisition system) are given in [7]. We summarize here briefly the main characteristics.

The BGO detector has been designed to serve for several experiments scheduled at the LUNA underground facility [8]. It is shaped as a 28 cm long cylinder with a coaxial hole of 6 cm diameter. The radial thickness of the BGO is 7 cm. The crystal is optically divided into six sectors, each covering an azimuthal angle of 60 degrees. Two Hamamatsu R1847-07 photomultipliers (PMTs) are coupled to the opposite faces of each sector and can be read in coincidence reducing the electronic noise. The target chamber and the beam calorimeter are hosted inside the BGO hole (Fig. 1), where the center of the 10 cm long

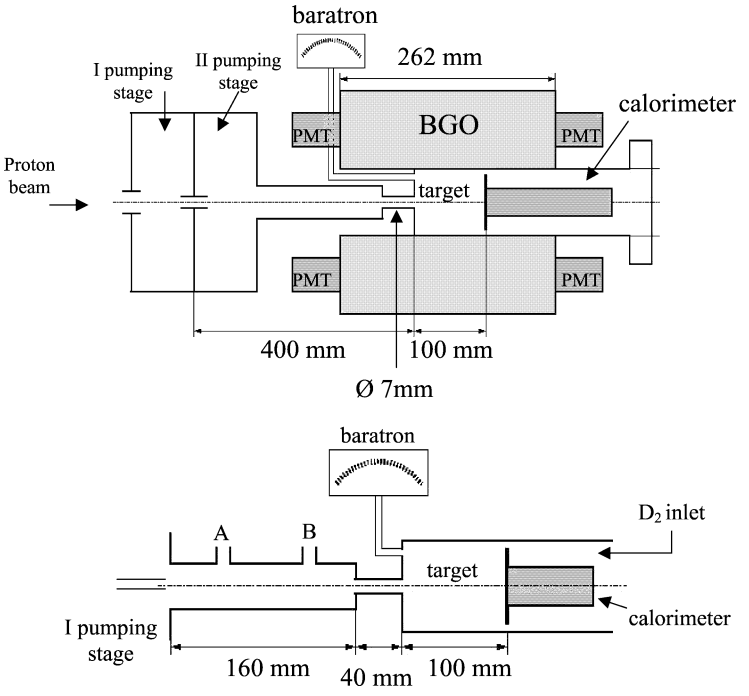

Fig. 1. Scheme of gas target set-up and BGO detector (top panel). In the bottom panel the geometry of the target zone and the points inside the first pumping stage, where the pressure profile was measured with an ad-hoc set-up with two apertures (labels A and B) are shown. Lengths in both panels are given in mm unit.

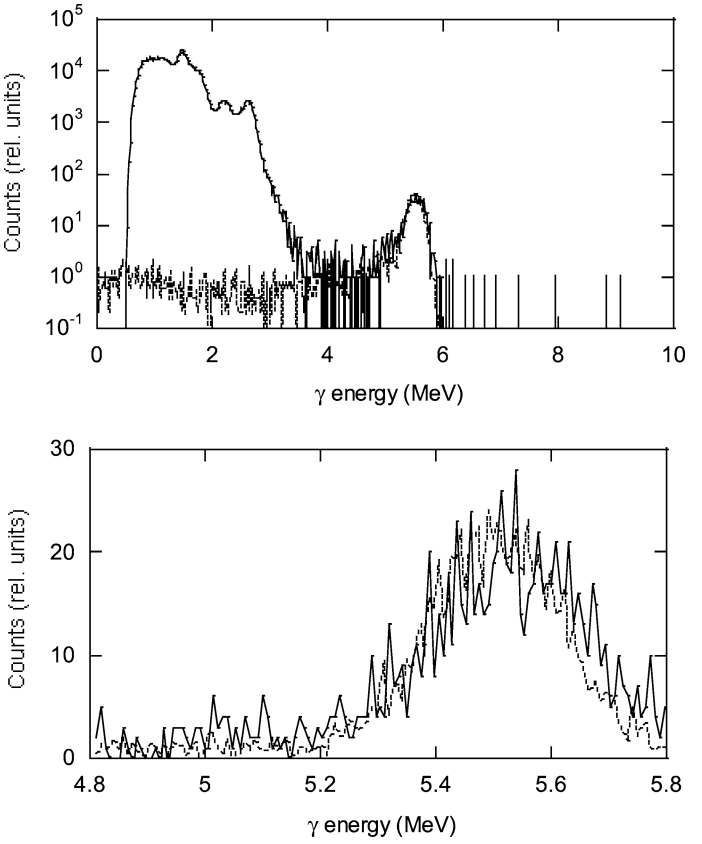

Fig. 2. Experimental (black line) and simulated (gray line) spectra of the 5.5 MeV photons from d(p, γ)^{3}He collected by the LUNA BGO detector for an interaction energy of 6.5 keV (center of the solar Gamow peak); nominal target pressure = 0.2 mbar. Spectra have been normalized to the maximum of d(p, γ)^{3}He peak. Top panel: full energy range; bottom panel: zoom of the region of interest for d(p, γ)^{3}He.

target cell is placed at the middle of the detector. This arrangement allows the detector to cover a large fraction of solid angle but heavily constrains the dimensions of the calorimeter itself. The detection efficiency for 5.5 MeV γ-rays is about 70% with an energy resolution in the total absorption peak of 8%. In Fig. 2, a measured spectrum of the γ-rays produced by d(p, γ)^{3}He is compared with a simulation by the LUNA Monte Carlo code [9]. In the experimental spectrum the contribution of natural radioactive isotopes (^{226}Ra, ^{40}K, ^{208}Tl) is visible below $E_\gamma = 3$ MeV. The angular distribution of emitted γ-rays described in [6] has been assumed in the simulations. We fixed $S_{\text{s-wave}}(E = 0) = 0.109$ eV b and $S_{\text{p-wave}}(E = 0) = 0.073$ eV b, as reported in [6]. We made simulations varying these values within the uncertainties reported in [6] and the detection efficiency turned out constant within 0.5%. Moreover, using the angular distribution given in [5] the change in efficiency was again lower than 1%.

The beam enters the target chamber of the differentially pumped gas-target system (three pumping stages) through apertures of high gas flow impedance: the collimator just before the target cell is 40 mm long with a diameter of 7 mm. The pressure of deuterium gas in the target chamber is measured by a Baratron capacitance manometer to an accuracy of better than 1%. The pressure in the target chamber is kept constant using a needle valve in combination with an electronic regulation unit. Tests have been performed [7] to check the homogeneity of the pressure profile inside the 10 cm long target and to control possible pressure gradients along the 30 mm long pipe (Fig. 1) which connects the Baratron with the target chamber. In both cases no effects greater than 0.5% have been observed in the 0.1–0.5 mbar pressure range. The pressure profile in the first pumping stage has been measured through two apertures in a dedicated set-up (Fig. 1) and considered in the Monte Carlo simulations to evaluate the probability to producing and detecting γ-rays outside the target chamber (see below). The deuterium gas flowing out from the target chamber was compressed by roots blowers, cleaned efficiently using a zeolite adsorption trap (cooled to liquid nitrogen temperature), and fed back into the target chamber.

The beam current in the target chamber was determined using a beam calorimeter [7] with a constant temperature gradient between a "hot" side and "cold" side, which is maintained by a heater controlled by a LabVIEW program running on a PC. The use of a Faraday cup for this purpose is here prevented since in crossing the different stages of the gas-target system the charge state of low energy projectiles fluctuates [10]. The power delivered by the beam (and consequently the number of projectiles) is deduced as the difference between the heating power without beam ($W_{\text{zero}} \cong 4$ W) and with beam (W_{run}). Thus, the number of projectiles, N_{p}, impinging on the calorimeter per unit time is given by

$$N_{\text{p}} = \frac{(W_{\text{zero}} - W_{\text{run}})}{E_{\text{cal}}}, \tag{2}$$

where E_{cal} is the laboratory energy of the beam projectiles when they arrive at the calorimeter. This energy is calculated by the LUNA Monte Carlo code [9] according to tabulations of stopping power [11]. The calorimeter has been designed to measure with good precision beam powers in the range 0.2–3 W. It has been directly calibrated at the 50 kV LUNA accelerator [7] within a systematic uncertainty of 1%. At the very low energies reached in the experiment, the extraction efficiency from the ion source is low and the beam power rapidly approaches the calorimeter limit ($W_{\text{zero}} \cong W_{\text{run}}$): the corresponding uncertainty on N_{p} gives the major contribution to the accidental error on the reaction cross section. To increase the beam current we tuned the analyzing magnet to select different beams: H_1^+, H_2^+ and H_3^+. In fact the extraction efficiency turned out to be higher for the molecular beams H_2^+ and H_3^+.

3. Data analysis

The proton beam looses part of its energy passing through the sections of the gas-target system. The reaction cross section is thus varying along the target length and the number of target atoms is also changing according to the deuterium pressure profile along the beam

path. Fusion reactions can therefore take place, with different probability, not only inside the 10 cm long target chamber but also in the previous stages of the system (Fig. 1) and the emitted 5.5 MeV photons can be detected by the BGO with an efficiency depending on the interaction position. With the coordinate z along the beam path, the number of detected photons, N_γ, is given by

$$N_\gamma = N_\mathrm{p} \frac{M}{kT} \int_0^L p(z)\sigma\big(E(z)\big)\eta(z)\,\mathrm{d}z, \tag{3}$$

where N_p is defined above, M is the number of atoms per molecule of the D_2 target gas, k is the Boltzmann constant, T the gas temperature, $p(z)$ the gas pressure at z, σ the cross section, and η the detection efficiency (see later). The length $L = 30$ cm (see Fig. 1) is the distance between the second collimator, in the first pumping stage, and the calorimeter: it corresponds to the gas-target zone where fusion reactions can take place and can be detected by the BGO with a probability greater than 0.1%. Thus $Mp(z)/(kT)$ is the number of target atoms per unit length. The laboratory energy of the projectiles at z is given by

$$E_\mathrm{p}(z) = E_\mathrm{extr} - \int_0^z \frac{\mathrm{d}E}{\mathrm{d}z}\,\mathrm{d}z, \tag{4}$$

where E_extr is the laboratory energy of the projectiles at extraction from the ion source and $\mathrm{d}E/\mathrm{d}z$ is the energy loss of protons in the deuterium gas [11]. According to (1), the cross section of $\mathrm{d}(\mathrm{p},\gamma)^3\mathrm{He}$ is expected to be continuously varying at low energies and we can extract from (3) an *effective* cross section, σ_eff, which is the average over the interaction energies:

$$\sigma_\mathrm{eff} = \frac{N_\gamma}{N_\mathrm{p}\frac{M}{kT}\int_0^L p(z)\eta(z)\,\mathrm{d}z}. \tag{5}$$

From (5) one can deduce the $S(E)$ factor, according to definition (1), provided that an average interaction energy, $E = E_\mathrm{eff}$, is introduced. This quantity, together with the projectile energy at the calorimeter, E_cal, and the integral in (5) is calculated by the LUNA Monte Carlo code [10]: it is the average value of the interaction energy of the detected capture reactions. We checked that this definition corresponds within 1%, with the standard approach [1] where E_eff is the energy for which the average value of σ, over the interval of the interaction energies, is σ_eff.

The number of detected events, N_γ, is obtained from the BGO spectra: for each trigger (OR of the coincidences among the six pairs of PMTs) the acquisition system [7] stores on a tape the pulse heights of all the 12 PMTs. The tapes are analyzed off-line to reconstruct, event by event, the energy deposition in the BGO sectors: a photon is counted when the sum of the six sector signals falls between 4.8 and 5.8 MeV. This Region Of Interest (ROI) has been defined by the maximum ratio between detection efficiency and background counts. In the ROI the BGO background at LNGS, without any passive shielding, is 30 ± 3 counts/day, about six orders of magnitude lower than the rate measured at the earth surface [7]. The N_γ quantity, for each run, is the net count in the ROI after background

subtraction. In the energy range explored in this experiment the counting rate ranged from 2000 counts/h ($E = 21$ keV) to 50 counts/day ($E = 2.5$ keV).

The number of projectiles, N_p, is deduced from (2): its uncertainty depends on those of W_{zero}, W_{run} and E_{cal}. During the experiment W_{zero} was constantly monitored and we observed a 0.8% (standard deviation) fluctuation of values due to accidental variation of heat transfer conditions of the calorimeter components. We attributed this error to the W_{zero} values measured after each run; the same uncertainty was attributed to the W_{run} values. At the lowest beam energies these very small fluctuations of the heating power (typical W_{zero} values were around 4 W), due to the difference in (2), resulted in a large uncertainty of the beam power. Fig. 3 shows the decrease of maximum beam power with beam energy and the corresponding increase of the calorimeter measurement uncertainty. The E_{cal} quantity is affected by a 10% systematic uncertainty of the stopping powers as quoted in [11]. Actually, $E_{cal} = E_{extr} - \Delta_{Ecal}$, where the last term indicates the total energy loss of the beam along the gas-target system: due to the optimum beam energy definition of the LUNA accelerator only the 10% uncertainty on Δ_{Ecal} is significant. At the different beam energies

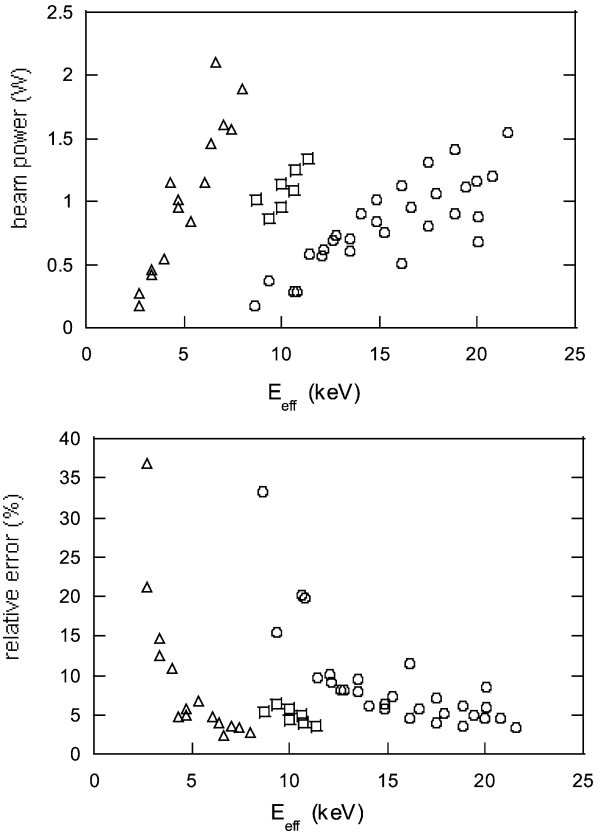

Fig. 3. Beam power delivered to the calorimeter (top) and its percentage uncertainty (bottom) as function of the interaction energy during the d(p, γ)^{3}He experiment (circles: H_1^+ beam; squares: H_2^+ beam; triangles: H_3^+ beam).

and target pressures used for the experiment, the systematic uncertainty on $E_{\rm cal}$ ranges from 0.1% ($E_{\rm extr} = 34$ keV, $p = 0.1$ mbar) to 2% ($E_{\rm extr} = 3$ keV, $p = 0.3$ mbar).

The integral in (5) was calculated by the LUNA Monte Carlo code for the different conditions of the experiment (i.e. beam energy and target pressure). The code received as input the measured pressure profile along the beam path: in the pipe sections where direct pressure measurements where impossible (for example inside the 40 mm long collimator at the target entrance) linear pressure gradients have been assumed. We always found a linear relation between the integral in (5) and the beam energy as shown in Fig. 4. It should be noted that, depending on the nominal target pressure (set point of the needle valve), the fraction of detected γ-rays produced in reactions outside the target chamber varies between 0.5% and 1.5%. The simulation results are affected by a 2% systematic error due to the approximation introduced in the description of the system geometry and pressure profile; a further systematic 1% uncertainty comes from the Baratron calibration. Other accidental uncertainties on the cross section calculation are 1% on the Baratron readings and 1% on the gas temperature (a maximum ± 3 K fluctuation in the laboratory temperature has been considered).

The Monte Carlo code gives also the average interaction energy $E = E_{\rm eff}$, that means the average of the distribution of reaction energies for the events detected in the ROI of the BGO spectra. $E_{\rm eff}$ has been calculated as a function of beam energy and target pressure obtaining linear fits adopted for the data reduction (Fig. 5): an example of the distribution of the interaction energies is presented in Fig. 6. It should be noted that standard deviations of these distributions turned out always about 1% of their averages. $E_{\rm eff}$ is affected, as $E_{\rm cal}$, by the systematic uncertainty of the stopping powers [11]: since $E_{\rm eff}$ is inside the exponential term in Eq. (1) its uncertainty affects the astrophysical $S(E)$ factor according to the equation

$$\left(\frac{\Delta S}{S}\right) = \sqrt{\left(\frac{\Delta\sigma}{\sigma}\right)^2 + \left(1 - \sqrt{2}\pi\,\frac{Z_1 Z_2 e^2}{2\eta}\sqrt{\frac{\mu}{E_{\rm eff}}}\right)^2 \left(\frac{\Delta E_{\rm eff}}{E_{\rm eff}}\right)^2}. \tag{6}$$

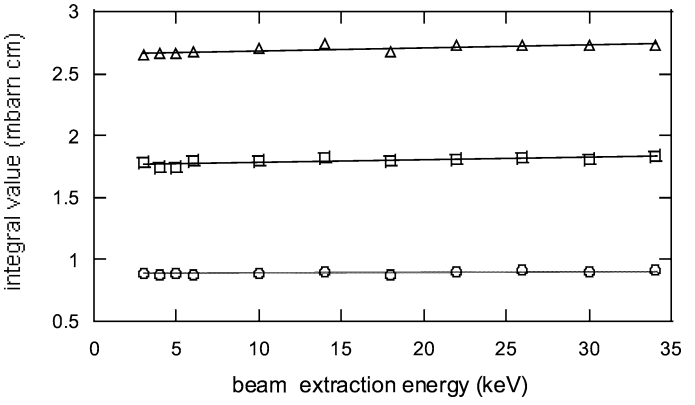

Fig. 4. The values of the integral in (5), for target pressure of 0.1 (circles), 0.2 (squares) and 0.3 (triangles) mbar versus the beam extraction energy as evaluated by the LUNA Monte Carlo code. Linear fits adopted for the data reduction are also shown.

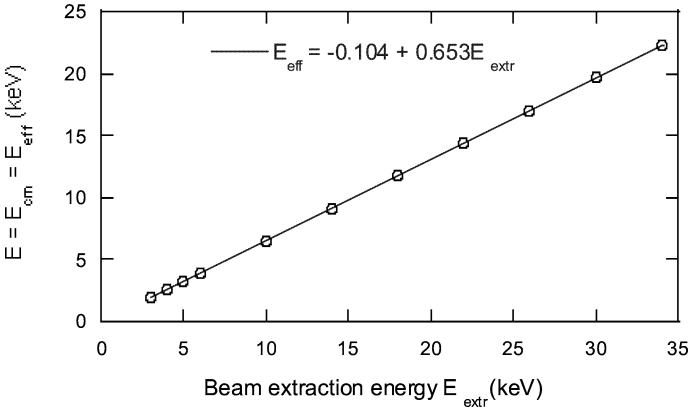

Fig. 5. Mean c.m. interaction mean energy, $E_{\rm eff}$, versus beam extraction energy at a target pressure of 0.2 mbar as calculated by the LUNA Monte Carlo code. The fitting equation has been used in the data reduction: a similar analysis gives $E_{\rm eff} = -0.056 + 0.657 E_{\rm extr}$ and $E_{\rm eff} = -0.150 + 0.650 E_{\rm extr}$ at 0.1 and 0.3 mbar, respectively.

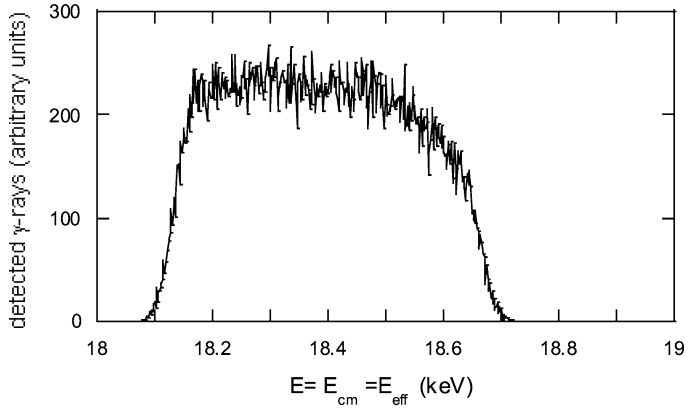

Fig. 6. Interaction energy distribution in c.m., $E_{\rm eff}$, calculated by the LUNA Monte Carlo for a beam extraction energy (in the laboratory system) of 29.29 keV and a nominal target pressure of 0.2 mbar: mean = 18.38 keV, standard deviation = 0.25 keV.

At the lowest energy reached in the experiment ($E_{\rm eff} = 2.58$ keV, $p = 0.3$ mbar) the systematic uncertainty on $E_{\rm eff}$ is 0.6% which produces, according to (6), a 4.7% contribution to the error on $S(E)$. This is negligible compared with the accidental uncertainty on the cross section in the same conditions (43%, mainly depending on beam power measurement and counting statistics; see Table 1).

4. Results

We measured the $\mathrm{d(p,\gamma)^3He}$ cross section varying the extraction beam energy between 32 and 4 keV in fine steps. The results are summarized in Table 1 (and represented in

Fig. 7) where the cross section and $S(E)$ values are listed for all experimental runs. In Table 1 only accidental errors are reported: the systematic uncertainties ranged from 3.6% ($E_{\rm eff} = 21.23$ keV, highest measured energy) to 5.3% ($E_{\rm eff} = 2.52$ keV, lowest measured energy) and are negligible in comparison with the accidental errors. During the experiment we changed the target pressures and we utilized different molecular beams (H_1^+, H_2^+, H_3^+): no systematic effects due to these parameters could be observed in the data (Table 1).

At the center of the solar Gamow peak ($E = 6.5$ keV) the S-factor turned out to be $0.26 \pm 0.01(\text{acc}) \pm 0.01(\text{sys})$ eV b. The S-factor data show a linear trend with the interaction energy as expected since both s-wave and p-wave captures contribute to the cross section value [5,6]. LUNA data can be compared with those obtained in previous experiments [5,6] as shown in Fig. 8: it turns out that the measured S-factor in the Gamow peak region is in agreement with the extrapolation from higher-energy data reported in [6]. The older experiment [5] found, in its measured energy range, a 40% higher S-factor.

The S-factor at zero energy, $S(0)$, can also be compared (Table 2) with the prediction of a recent model [12] and its extrapolation reported in [5,6]. The LUNA data extrapolation is again in agreement, at a 3σ level, with [6] and with the model [12], but it should be noted that for the LUNA data the extrapolation to zero-energy region is 2.5 keV only. The

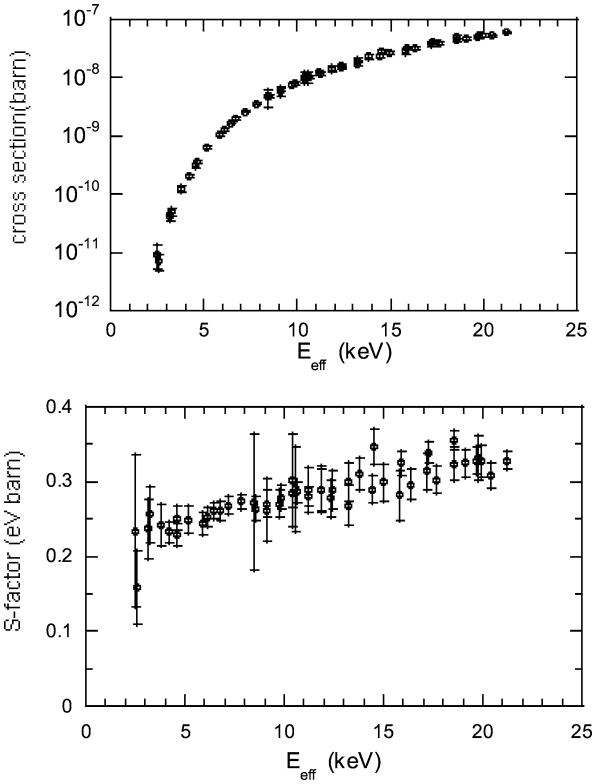

Fig. 7. Cross section (top) and S-factor (bottom) values obtained as function of the interaction energy $E_{\rm eff}$.

Table 1
Measured cross section and astrophysical S-factor values as functions of the extraction beam energy ($E_{\rm extr}$, in the laboratory) and of the effective interaction energy ($E_{\rm eff}$). Only accidental uncertainties are quoted in the table

$E_{\rm extr}$ (keV)	$E_{\rm eff}$ (keV)	$\sigma_{\rm eff}$ (b)	$\Delta\sigma_{\rm eff}$ (b)	S (eV b)	ΔS (eV b)
4.04	2.52[c,f]	9.2×10^{-12}	4.0×10^{-12}	2.30×10^{-1}	1.0×10^{-1}
4.05	2.58[b,f]	7.2×10^{-12}	2.2×10^{-12}	1.59×10^{-1}	4.9×10^{-2}
5.04	3.16[c,f]	4.12×10^{-11}	7.0×10^{-12}	2.37×10^{-1}	4.0×10^{-2}
5.04	3.22[b,f]	5.00×10^{-11}	7.4×10^{-12}	2.56×10^{-1}	3.8×10^{-2}
6.04	3.81[c,f]	1.25×10^{-10}	1.5×10^{-11}	2.42×10^{-1}	2.9×10^{-2}
6.50	4.18[b,f]	1.98×10^{-10}	1.1×10^{-11}	2.33×10^{-1}	1.3×10^{-2}
7.09	4.56[b,f]	3.07×10^{-10}	2.0×10^{-11}	2.29×10^{-1}	1.5×10^{-2}
7.07	4.63[a,f]	3.63×10^{-10}	2.2×10^{-11}	2.51×10^{-1}	1.5×10^{-2}
8.05	5.19[b,f]	6.23×10^{-10}	4.4×10^{-11}	2.49×10^{-1}	1.8×10^{-2}
9.06	5.85[b,f]	1.034×10^{-9}	6.4×10^{-11}	2.43×10^{-1}	1.5×10^{-2}
9.60	6.11[c,f]	1.295×10^{-9}	6.6×10^{-11}	2.52×10^{-1}	1.3×10^{-2}
9.98	6.46[b,f]	1.684×10^{-9}	6.7×10^{-11}	2.62×10^{-1}	1.1×10^{-2}
10.56	6.74[c,f]	1.98×10^{-9}	9.6×10^{-11}	2.61×10^{-1}	1.3×10^{-2}
11.10	7.19[b,f]	2.63×10^{-9}	1.1×10^{-10}	2.69×10^{-1}	1.1×10^{-2}
12.01	7.80[b,f]	3.60×10^{-9}	1.3×10^{-10}	2.73×10^{-1}	9.7×10^{-3}
12.98	8.43[b,d]	4.7×10^{-9}	1.6×10^{-9}	2.73×10^{-1}	9.17×10^{-2}
13.10	8.51[b,e]	4.73×10^{-9}	3.0×10^{-10}	2.64×10^{-1}	1.7×10^{-2}
14.01	9.11[b,d]	5.89×10^{-9}	9.5×10^{-10}	2.62×10^{-1}	4.2×10^{-2}
14.04	9.13[b,e]	6.13×10^{-9}	4.2×10^{-10}	2.71×10^{-1}	1.9×10^{-2}
14.95	9.73[b,e]	7.49×10^{-9}	5.0×10^{-10}	2.70×10^{-1}	1.8×10^{-2}
14.95	9.84[a,e]	7.98×10^{-9}	4.5×10^{-10}	2.79×10^{-1}	1.6×10^{-2}
15.90	10.36[b,d]	1.00×10^{-8}	2.1×10^{-9}	3.01×10^{-1}	6.2×10^{-2}
15.94	10.38[b,e]	9.61×10^{-9}	6.4×10^{-10}	2.85×10^{-1}	1.9×10^{-2}
16.18	10.55[b,d]	1.02×10^{-8}	2.0×10^{-9}	2.90×10^{-1}	5.8×10^{-2}
16.11	10.62[a,e]	1.022×10^{-8}	5.2×10^{-10}	2.86×10^{-1}	1.5×10^{-2}
17.18	11.21[b,d]	1.21×10^{-8}	1.3×10^{-9}	2.88×10^{-1}	3.0×10^{-2}
17.03	11.23[a,e]	1.183×10^{-8}	5.7×10^{-10}	2.80×10^{-1}	1.4×10^{-2}
18.15	11.85[b,d]	1.42×10^{-8}	1.5×10^{-9}	2.90×10^{-1}	3.1×10^{-2}
18.20	11.87[b,d]	1.42×10^{-8}	1.4×10^{-9}	2.89×10^{-1}	2.8×10^{-2}
18.90	12.34[b,d]	1.51×10^{-8}	1.3×10^{-9}	2.77×10^{-1}	2.4×10^{-2}
19.18	12.39[c,d]	1.60×10^{-8}	1.4×10^{-9}	2.89×10^{-1}	2.5×10^{-2}
20.23	13.22[b,d]	1.96×10^{-8}	1.6×10^{-9}	3.00×10^{-1}	2.5×10^{-2}
20.23	13.22[b,d]	1.75×10^{-8}	1.7×10^{-9}	2.68×10^{-1}	2.7×10^{-2}
21.12	13.81[b,d]	2.26×10^{-8}	1.6×10^{-9}	3.11×10^{-1}	2.2×10^{-2}
22.24	14.42[c,d]	2.34×10^{-8}	1.5×10^{-9}	2.90×10^{-1}	1.9×10^{-2}
22.24	14.55[b,d]	2.86×10^{-8}	2.0×10^{-9}	3.46×10^{-1}	2.4×10^{-2}
22.87	14.97[b,d]	2.64×10^{-8}	2.1×10^{-9}	2.99×10^{-1}	2.4×10^{-2}
24.16	15.82[b,d]	2.82×10^{-8}	3.4×10^{-9}	2.82×10^{-1}	3.4×10^{-2}
24.25	15.89[b,d]	3.28×10^{-8}	1.6×10^{-9}	3.25×10^{-1}	1.6×10^{-2}
24.92	16.33[b,d]	3.18×10^{-8}	2.1×10^{-9}	2.96×10^{-1}	2.0×10^{-2}
26.25	17.21[b,d]	3.77×10^{-8}	3.0×10^{-9}	3.14×10^{-1}	2.5×10^{-2}
26.28	17.23[b,d]	4.07×10^{-8}	1.6×10^{-9}	3.39×10^{-1}	1.4×10^{-2}
26.88	17.63[b,d]	3.82×10^{-8}	2.3×10^{-9}	3.02×10^{-1}	1.8×10^{-2}
28.26	18.54[b,d]	4.52×10^{-8}	3.1×10^{-9}	3.24×10^{-1}	2.2×10^{-2}
28.29	18.56[b,d]	4.97×10^{-8}	1.9×10^{-9}	3.55×10^{-1}	1.4×10^{-2}

(*continued on next page*)

Table 1 (*continued*)

E_{extr} (keV)	E_{eff} (keV)	σ_{eff} (b)	$\Delta\sigma_{eff}$ (b)	S (eV b)	ΔS (eV b)
29.10	19.10[b,d]	4.81×10^{-8}	2.7×10^{-9}	3.25×10^{-1}	1.9×10^{-2}
29.95	19.66[b,d]	5.14×10^{-8}	2.8×10^{-9}	3.28×10^{-1}	1.8×10^{-2}
30.09	19.91[a,d]	5.25×10^{-8}	3.5×10^{-9}	3.28×10^{-1}	2.2×10^{-2}
30.11	19.77[b,d]	5.25×10^{-8}	4.8×10^{-9}	3.32×10^{-1}	3.1×10^{-2}
31.10	20.43[b,d]	5.19×10^{-8}	2.8×10^{-9}	3.09×10^{-1}	1.7×10^{-2}
32.31	21.23[b,d]	5.92×10^{-8}	2.2×10^{-9}	3.28×10^{-1}	1.2×10^{-2}

[a] Runs with a nominal target pressure of 0.1 mbar.
[b] Runs with a nominal target pressure of 0.2 mbar.
[c] Runs with a nominal target pressure of 0.3 mbar.
[d] Runs with H_1^+ beam.
[e] Runs with H_2^+ beam.
[f] Runs with H_3^+ beam.

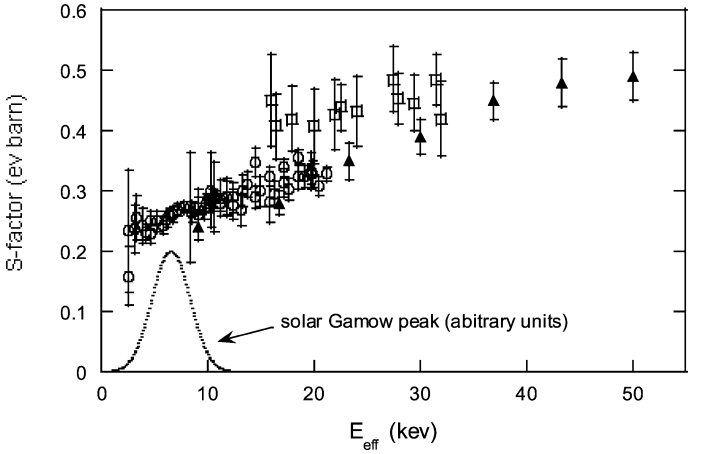

Fig. 8. S-factor data and linear fits for the d(p, γ)^{3}He reaction from [5] (squares), [6] (full triangles) and present work (circles). The position of the solar Gamow peak is also shown schematically.

comparison with [5] is less significative if the quite large uncertainty of $S(0)$ quoted in that paper is considered.

Electron screening effects can be estimated for this reaction assuming standard approaches: in the adiabatic approximation [13] the expected enhancement of the S-factor at 2.5 keV (c.m.) is about 6% and it increases to 20% for interaction energies around 1 keV. The precision of our data prevents any estimation, even qualitative, of the effect. Moreover, an experiment addressed to this study should improve the luminosity by about two orders of magnitude (Fig. 3) and this seems not achievable in the near future.

Table 2
S-factor linear fit parameters S_0 and S_0', where $S(E) = S_0 + S_0' E_{\mathrm{c.m.}}$, reported in [5,6], and the extrapolated S-factor at zero energy, $S(0)$, deduced in a theoretical paper [11] compared with the results of this experiment. Values from [5,6,12] are as reported by the authors

Authors	S_0 (eV b)	S_0' (eV b keV^{-1})	$S(0)$ (eV b)
Schiavilla et al. [12]	–	–	0.185 ± 0.005
Griffiths et al. [5]	–	–	0.25 ± 0.04
Schimd et al. [6]	0.166 ± 0.005	0.0071 ± 0.0004	0.166 ± 0.014
Present work	0.216 ± 0.006	0.0059 ± 0.0004	0.216 ± 0.010

5. Conclusions

The LUNA collaboration, thanks to the technical solution developed for a new high sensitivity gas-target set-up and to the low background conditions at LNGS, has performed the first measurement of the d(p, γ)^{3}He reaction in the energy range of the solar Gamow peak and near that in proto-stars. This is the second time following the ^{3}He(^{3}He, 2p)^{4}He experiment [3], that a reaction of the p–p chain has been directly studied in the proper energy range without any extrapolation from higher energies. The set-up will be utilized in the near future for other experiments on radiative capture reactions of the p–p chain and CNO cycle.

Acknowledgements

We are indebted for the skill support of the INFN technical staff at Genoa, LNGS, and Naples.

References

[1] C. Rolfs, W.S. Rodney, Cauldrons in the Cosmos, University of Chicago Press, Chicago, 1988.
[2] U. Greife et al., Nucl. Instrum. Methods A 350 (1994) 327.
[3] R. Bonetti et al., Phys. Rev. Lett. 82 (1999) 5205.
[4] S.W. Stahler, Astrophys. J. 332 (1988) 804.
[5] G.M. Griffiths, M. Lal, C.D. Scarfe, Can. J. Phys. 41 (1963) 724.
[6] G.J. Schmid et al., Phys. Rev. C 56 (1997) 2565.
[7] C. Casella et al., A new setup for the underground study of capture reactions, Nucl. Instrum. Methods A, in press.
[8] P. Prati et al., Nucl. Phys. A 654 (1999) 920c.
[9] C. Arpesella et al., Nucl. Instrum. Methods A 360 (1995) 607.
[10] S.K. Allison, Rev. Mod. Phys. 30 (1958) 1138.
[11] J.F. Ziegler, Program TRIM-91, The Transport of Ions in Matter, IBM Research, New York, 1991.
[12] R. Schiavilla, M. Viviani, A. Kievsky, Phys. Rev. C 54 (1996) 553.
[13] H.J. Assenbaum et al., Z. Phys. A 327 (1989) 461.